Efficient Multiplexed Label-free Detection by Flexible MXene/Graphene Oxide Fibers with Enhanced Charge Transfer and Hot Spots Effect

Xin Liu[1,2], *Alei Dang*[1,2]*, *Tiehu Li*[1,2]*, *Yiting Sun*[1,2], *Weibin Deng*[1,2], *Tung-Chun Lee*[3], *Yong Yang*[1], *Amir Zada*[4], *Boning Wang*[1], *Yuhui Liu*[1,2], *Shaoheng Wu*[1,2] *Tingkai Zhao*[1,2]

[1.] School of Materials Science and Engineering, Northwestern Polytechnical University, Xi'an 710072, P. R China.

[2.] Shannxi Engineering laboratory for Graphene New Carbon Materials and Applications, School of Materials Science and Engineering, Northwestern Polytechnical University, Xi'an 710072, P. R China.

[3.] Department of Chemistry, University College London (UCL), London WC1H 0AJ, U.K.

[4.] Department of Chemistry, Abdul Wali Khan University, Mardan, Khyber Pakhtunkhwa, 23200, Pakistan

[*]Corresponding author: Alei Dang, Tiehu Li

E-mail address: dangalei@nwpu.edu.cn; litiehu@nwpu.edu.cn

Abstract: Sensors integrated with sampling and analysis processes are the key in analytical chemistry, environmental protection and national security. However, achieving reliable and sensitive large-scale rapid screening of target analytes is still challenging. Herein, we demonstrate a robust surface-enhanced Raman scattering (SERS) sensor by constructing dense and uniform plasmonic hotspots on the flexible Ti_3C_2Tx MXene/graphene oxide (MG) fibers through a self-assemble strategy at the oil-water interface. The produced SERS substrates exhibited an ultralow limit of detection (LOD, 1×10^{-15} M for R6G), outstanding sensitivity (EF = 1.53×10^{12}) and high stability for R6G molecules (RSD = 9.47%, over 60 days storage). SERS experiments and theoretical simulations suggested that acidified Ti_3C_2Tx MXene further excited charge-transfer (CT) resonance of the system, while the assembled Ag nanostructures produced a large electromagnetic (EM) field enhancement. Thus, the fiber sensor not only realizes the multiplexed and powerful detection of pesticide residues (LOD of 10^{-11} M) with an error < 7.3% via an established concentration-dependent standard color barcodes, but also allows the recognization of target molecules in a wide range of fields, such as methylene blue, crystal violet and nikethamide. This work provides new insights in the development of versatile label-free sensors for the rapid multiplexed analysis of target molecules in real samples.

Keywords: Surface enhancement Raman Scattering, MXene, Ag nanoparticles, flexible substrate, multiplexed detection.

1. Introduction

Accurate molecular-level detection of the target molecules in real-world scenarios with good temporal and spatial scale is an end goal in a wide variety of fields ranging from analytical chemistry to environmental protection [1-4]. Several traditional techniques, including high-performance liquid chromatography (HPLC), gas chromatography (GC)[5], and enzyme-linked immunosorbent assays (ELISAs)[6] , have been used to evaluate target analytes with high sensitivity and accuracy. However, complex sample preparation methods and time-consuming analysis processes hinder the detection efficiency especially in the simultaneous identification of multicomponent analytes or large-scale screening[2]. Therefore, increasing efforts have been invested in developing a faster, more accurate and facile strategy.

Surface-enhanced Raman scattering (SERS), as a sensitive and nondestructive spectroscopic technique [2, 7-14] that avoids tedious sample preparation steps and time-consuming analysis processes, has shown potential services in the fields of analytical chemistry[15, 16], environmental protection[17, 18] and food safety[19]. In this context, a variety of SERS sensors with high activity have been manufactured for the detection of trace residues [20-23]. Compared to traditional rigid substrates, for instance, emerging flexible SERS substrates can collect pesticide molecules from complex surfaces by the swab sampling method[22, 24], and provide unprecedented efficiency and convenience for SERS detection in real samples[25, 26]. For example, Chen[24] *et al.* prepared an adhesive SERS tape for the rapid and sensitive detection of thiuram from the surface of vegetables. Wei[27] *et al.* achieved an in-situ detection of pollutants in fish scales by embedding SERS-active nanoparticles in a polymer film. However, although great progress has been made in polymer- or paper-based flexible SERS substrates, there are still several challenges to overcome. For instance, the low adhesion between polymers and precious metal nanoparticles makes it difficult to assemble plasmonic nanostructures on polymer surfaces. Although the embedded nanoparticles within the matrix can be used to improve stability, the formed structures lead to a

mismatch between the molecule and hot spots [19, 28]. Thus, it is still a challenge to fabricate a flexible SERS substrate with high sensitivity and stability in a large scale.

Two-dimensional (2D) transition metal carbides/nitrides (MXenes) have been explored as building blocks for SERS sensors[29-33] due to their low production cost, tunable electronic structure, and high carrier mobility [34-37]. MXene-based hybrid platforms and multidimensional plasmonic systems overcome many inherent limitations of SERS[38-40] and provide a new pathway towards practical sensing applications. For instance, Xie[41] *et al.* designed composite SERS substrates of MXene and Au nanorods for reliable and sensitive detection of organic pollutants. Yang[31] *et al.* loaded MXene nanosheets on the surface of a colloid-assembled 3D plasmonic nanostructures, enabling the detection of volatile organic compounds (VOCs) in air. However, these substrates are usually nanoscale or rigid, and are therefore difficult to apply for rapid in-situ sampling or large-scale screening. In our previous work[42], Ti_3C_2Tx MXene and plasmonic Au nanoclusters have been assembled into a flexible and highly reproducible SERS fibers. However, the low sensitivity and high cost of produced substrates limited their broad applicability in multiplexed label-free detection. Therefore, more efforts are needed to develop flexible Ti_3C_2Tx MXene-plasmonic nanoparticle composite SERS substrates with easy fabrication processes and well-defined hot spots.

Herein, we propose a strategy of combining wet-spinning and oil-water interface self-assembly method to construct flexible Ti_3C_2Tx MXene/graphene (MG) /Ag nanoparticles (AgNPs) fiber sensor with excellent SERS performance for the efficient multiplexed analysis of versatile target molecules. First, flexible MG fibers were prepared by wet spinning, and subsequently the surface of fiber was activated by an additional acidification process to improve the compatibility between the fiber and plasmonic hotspots. Thus, the uniform AgNPs were attached onto the surface of MG fibers by self-assembly at the oil-water interface for powerful SERS enhancement. As demonstrated by the SERS experiments and theoretical simulations, due to the dense electromagnetic hot spots of plasmonic nanostructures and the effective charge transfer of MXene, the flexible fiber sensor showed ultralow detection limits (1×10^{-15} M for

R6G), outstanding sensitivity (EF=1.53×10^{12}) and high stability (RSD=9.47%, stored at room temperature for more than 60 days). Moreover, the rapid multiplexed sensing of pesticide residues in fruit peels can be achieved with an error of less than 7.3% by virtue of the standard color barcode constructed from SERS spectra of flexible fiber substrates. Meanwhile, as a versatile label-free sensor, it also allows the recognization of MB (an organic pollutant), CV (a fish drug) and NTA (a prohibited stimulant) molecules in an efficient way.

2. Experimental Part

2.1 Materials

Rhodamine 6G ($C_{28}H_{31}N_2O_3Cl$, ≥99.0%), thiram ($C_6H_{12}N_2S_4$, ≥99.9%) and thiabendazole ($C_{10}H_7N_3S$, ≥99.9%) were purchased from Aladdin. Silver nitrate ($AgNO_3$, ≥99.99%), cyclohexane (C_6H_{12}, ≥99.99%), hydrochloric acid (HCl, 36~38%), nitric acid (HNO_3, 65%~68%), graphite powder (C, ≥99.85%), sulfuric acid (H_2SO_4, 95~98%), ethanol, calcium chloride ($CaCl_2$, ≥96.0%), potassium bromide (KBr, ≥99.9%), cetyltrimethyl ammonium bromide ($C_{19}H_{42}BrN$, CTAB, ≥99.9%), polyvinyl pyrrolidone ($(C_6H_9NO)_n$, PVP, Mw=30000) and trisodium citrate ($C_6H_5Na_3O_7$, TSC, ≥99.9%) were purchased from Sinopharm Chemical Reagent Co., Ltd. (Shanghai, China). MAX phase Ti_3AlC_2 powder (300 mesh) was purchased from Laizhou Kaiene Ceramic Material Co., Ltd., and lithium fluoride (LiF, ≥99.0%) and pymetrozine ($C_{10}H_{11}N_5O$, ≥99.9%) were purchased from Macklin. Deionized water (homemade) was used throughout all the experiments. All reagents and materials were used directly without purification.

2.2 Preparation of MG and MG-Ox Fibers

MG fiber were prepared according to the previous report[43]. Briefly, graphene oxide nanosheets prepared by Hummers method were mixed with MXene nanosheets in a volume ratio of 1:9. The mixture was stirred at room temperature for more than 12 h and further centrifuged at 12500 rpm for 30 min to obtain a spinning solution (20 mg/mL). The spinning solution was extruded into a coagulation bath using a

microsyringe pump and collected on the reel. Finally, the fiber was soaked in deionized water for 12 h to remove excess impurities and dried at 60 °C under vacuum for 24 h. For the preparation of MG-Ox fiber, MG fiber was first immersed in a mixed acid solution of H_2SO_4 and HNO_3 with a volume ratio of 3:1 for 12 h and then washed and dried by the above method. Finally, the MG-Ox fiber was obtained.

2.3 Synthesis of AgNPs

AgNPs of 38.7 ± 4.1 nm diameter were synthesized according to Frens method. Typically, a mixture of 99 mL DI water and 1 mL of 0.1 M $AgNO_3$ was boiled in a round bottom flask followed by quick addition of 4 mL (1 wt%) TSC solution. For complete reduction of $AgNO_3$, the mixture was incubated for 1 h and then cooled to room temperature naturally. Finally, the excess surfactant was removed by centrifugation at 6000 rpm for 10 min. To prepare AgNPs capped with different functional groups, 1 mM aqueous solutions of KBr, TSC, PVP and CTAB were prepared. Then, the modified AgNPs were mixed with the above solutions in a 1:1 volume ratio and stirred at room temperature for 6 h. Finally, the AgNPs capped with different functional groups were separated from excess ligands/surfactants by centrifugation at 6000 rpm for 5 min and redispersed in ethanol solution for further use.

2.4 Assembly at the Oil-water Interface

AgNPs were assembled on the surface of MG-Ox fiber by an oil-water interface self-assembly technique. Briefly, a certain amounts of DI water and cyclohexane were added to a beaker to form an oil-water interface. MG-Ox fiber and 20 ml AgNPs were added to the oil-water mixture. After slowly adding a few drops of ethanol, the AgNPs spontaneously assembled on the fiber surface. For comparison, AgNPs were also transferred onto the Si wafer through a drop-casting method.

2.5 SERS Experiment

A series of R6G ethanol solutions (from 10^{-3} M~10^{-16} M) were used as probe molecules to study the SERS performance. In a typical process, 20 μL of R6G solution was dropped on the fiber surface, and a SERS test was performed after natural drying.

An Alpha300R confocal Raman microscope (WI Tec) equipped with a 532 nm (power = 0.1 mW) laser was used to collect Raman signals. The acquisition time was 15 s, and all SERS spectra were measured 3 times from at least 5 different positions of the samples to reduce the error. The same test method and parameter settings were also used in the detection of thiram, thiabendazole and pymetrozine ethanol solutions.

In the proof-of-concept experiment, 100 μL of pesticide solution in ethanol was first sprinkled on the peach and winter jujube and dried at room temperature. The flexible fibers stained with ethanol were wiped on the peel surface several times to collect pesticide residues. Finally, the fibers were dried at room temperature, and SERS spectra were measured by Raman microscopy.

2.6 Characterization

The morphology and structure of the fibers and AgNPs were examined with scanning electron microscopy (SEM, Verios G4, 5 kV). An X-Pert PRO X-ray diffractometer (Cu Kα1, λ=0.154 nm) was employed to detect and analyze the crystal structure of the samples. To clarify the optical performance of the samples, UV–Vis spectroscopic measurements were performed with a TU-1810PC UV–vis spectrometer (Persee, Beijing). Moreover, a zeta potentiometer (Zeta Sizer Nanozs, Malvern) was used to measure the zeta potential of MXene and the capped AgNPs with different functional groups. X-ray photoelectron spectroscopy (XPS, Thermo Scientific TM K-Alpha TM+ spectrometer) equipped with an Al Kα X-ray source was performed to characterize the valence state of each element, and all peaks were calibrated with the C1 s peak binding energy at 284.8 eV.

2.7 Finite Element Method Electromagnetic Simulation

The electromagnetic field simulation was run in the COMSOL electromagnetics module. The incident wavelength was defined as 532 nm, and the dielectric constant and refractive index of all materials were provided by the software. The positions of AgNPs were set at the vertices and the center of the hexagon and parallel with the MXene nanosheets. All outside boundaries were regarded as perfectly matched

boundary layers (PMLs) to achieve absorbing boundary conditions, and ultrafine grids were used to improve the calculation accuracy.

2.8 First-principles Calculations

Density functional theory (DFT) was employed to investigate the band structure and electronic properties of MXene using the CASTEP program in Materials Studio. During the calculation process, the Perdew-Burke-Ernzerhof (PBE) functional in the generalized gradient approximation (GGA) was used to describe the exchange-correlation energy and the boundary conditions. The cutoff energy of the plane wave was chosen as 500 eV, and Monkhorst-Pack vector grid k-points were set to $6\times6\times2$. The convergence tolerance for the total energy of the system was set to 10^{-5} eV/atom, and the force acting on each atom was less than 0.03 eV/Å.

3. Results and Discussion

MG fiber with high flexibility was prepared through the wet-spinning method according to previous work[43]. **Figure 1a** shows a typical MG-Ox fiber fabrication process. In the first step, few layers of MXene nanosheet (2.94 nm) with high crystallinity (**Figure S1**) were synthesized by selective etching of Al in Ti_3AlC_2 (MAX phase). However, due to the weak interlaminar force between the nanosheets, pure MXene are difficult to assemble on the fiber with high flexibility and a meter-scale length. With this in mind, graphene oxide (GO) was used as templates to promote the spin ability of Ti_3C_2Tx MXene due to its excellent liquid crystal properties. However, excessive GO additions can lead to a decrease in SERS performance (**Figure S2**). Therefore, we have chosen a GO addition of 10 wt% to balance the spinning and SERS performance. Briefly, the formed spinning solution from MXene/GO (MG) hybrid nanosheets were shaped by a 26 G microneedle during the wetting spinning process, and subsequently the as-synthesized MG fiber was solidified in a coagulation bath and collected on the reels continuously. The produced MG fiber demonstrated an excellent flexibility under the action of combined the ionic bonds and van der Walls forces between nanosheets, making it a good candidate for flexible SERS sensor. To assist the

self-assembly of AgNPs on MG fiber at the oil-water interface and enhance their interfacial bonding force, an additional acidification step was used to modify the MG fiber. After the treatment of the MG fiber by a mixed solution of H_2SO_4 and HNO_3, acidified MG fiber (MG-Ox) were fabricated. **Figure 1b** and **c** shows the surface morphology of MG fiber before and after acidification. Compared to the MG fiber, a clearer axial alignment of MG nanosheets and deeper grooves can be observed on the surface of MG-Ox fiber, which endows the different assembled nanostructure of AgNPs and their corresponding SERS performance [7, 44].

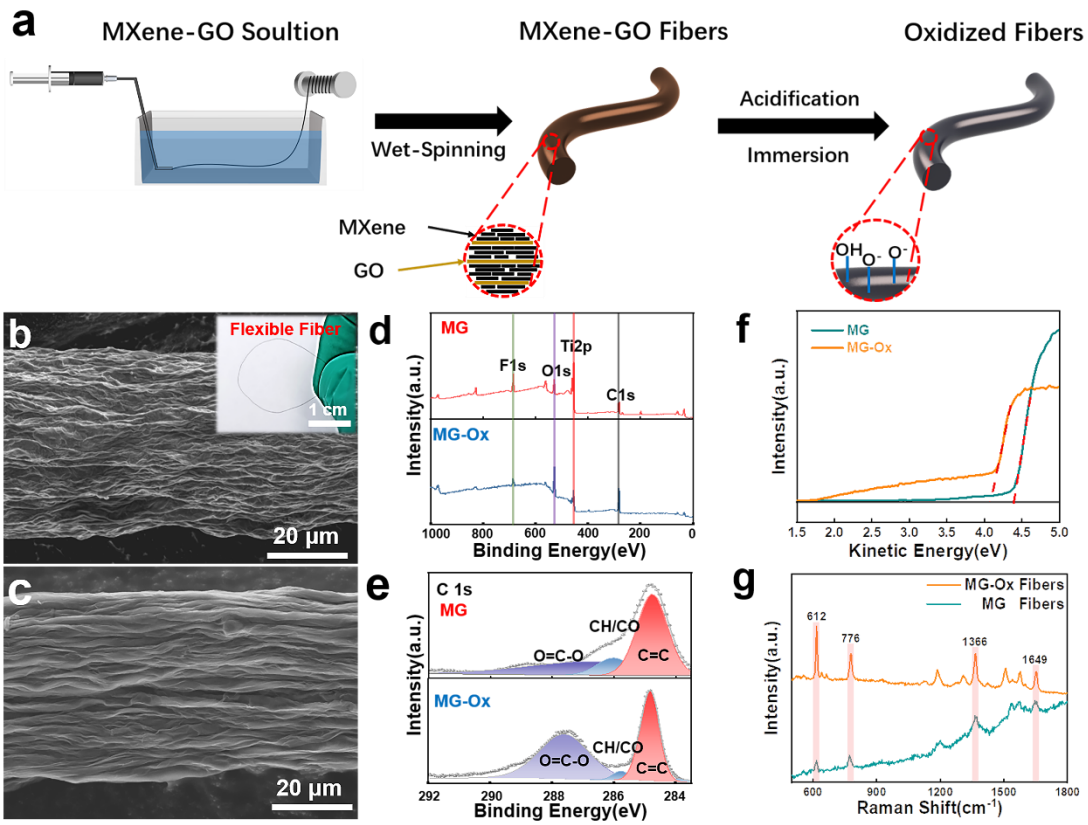

Figure 1. (a) Schematic illustration of the of MG-Ox fiber by wet spinning and acidification methods. SEM images of (b) MG and (c) MG-Ox fibers, and their corresponding XPS survey spectra (d) and high-resolution C1 s spectra (e). (f) UPS spectra of MG and MG-Ox fibers. (g) Raman signals collected from 1×10^{-5} M R6G on the surfaces of MG and MG-Ox fibers respectively. Inset in (b): the digital image of flexible MG fiber bended by hand.

X-ray photoelectron spectroscopy (XPS) was used to reveal the atomic chemical valence and bonding configurations of the MG and MG-Ox fibers. As illustrated in

Figure 1d and **Table S1**, the total XPS spectrum collected on the surface of fibers shows variation in the individual elements before and after acidification. Compared to the MG fiber, the contents of C and O elements in MG-Ox fiber increases from 13.95 At% and 19.90 At% to 32.51 At% and 36.87 At% respectively, while the content of Ti and F decreases from 42.19 At% and 23.96 At% to 19.14 At% and 11.48 At%. It indicates that the acidification process introduces a large number of oxygen-containing functional groups on the surface of MG fiber and replaces part of the original F group [35, 45]. These results are further supported by the shifting of the d (002) peak from 7.4° to 5.5° in the XRD spectra of MG and MG-Ox fibers (**Figure S3**), in which the introduction of oxygen-containing functional groups increases the interplanar spacing[37]. **Figure 1e** illustrates a comparison of the high-resolution XPS spectra of C1 s of MG and MG-Ox fibers. The C1 s peaks from both samples can be de-convoluted into C=C, CH/CO and O=C-O bonds at 284.8, 285.8 and 287.6 eV respectively. Compared with MG fiber, the intensity and area of the O=C-O peak of MG-Ox substantially increase, as verified by the high-resolution XPS spectra of O1 s (**Figure S4** and **Table S2**). It enables the surface of MG-Ox fiber to be more reactive for the assembly of dense plasmonic hotspots.

Moreover, UV photoelectron spectroscopy (UPS) was used to calculate the work function of MG and MG-Ox fibers. As shown in **Figure 1f**, the introduction of oxygen-containing functional groups reduces the work function of MG fiber from 4.39 to 4.08 eV, resulting in the charges more easily transferred from MG-Ox surface to the target molecules [32, 46]. To make this change clear, 1×10^{-5} M Rhodamine 6G (R6G) was used as a SERS probe molecule to investigate the SERS performance of MG and MG-Ox fibers. As demonstrated in **Figure 1g**, the Raman signals collected from MG-Ox fiber exhibit remarkable SERS effects whereas the Raman signals of the MG fiber are very weak for R6G. These exciting results display that the introduction of oxygen-containing functional groups not only increases the chemical activity of the fiber but also enhances the charge transfer (CT) ability and improves the SERS performance.

The AgNPs with an average diameter of 38.7 ± 4.1 nm (**Figure S5**) were employed to construct plasmonic nanostructures on the MG-Ox fiber surface by a self-assembly

approach at the oil-water interface, where the localized surface plasmonic resonance (LSPR) peak of AgNPs was found at around 421 nm (**Figure S5a**). Generally, monolayer Ag nanostructures can be fabricated at the cyclohexane/water interface based on the Marangoni effect[47] **(Figure S5b)** where the dispersed AgNPs in ethanol solvent can spontaneously rise from the bottom of the aqueous phase and accumulate at the oil-water interface due to the interfacial tension gradient, and produce a densely packed AgNPs plasmonic nanostructures (see details in the **Experimental Part**).

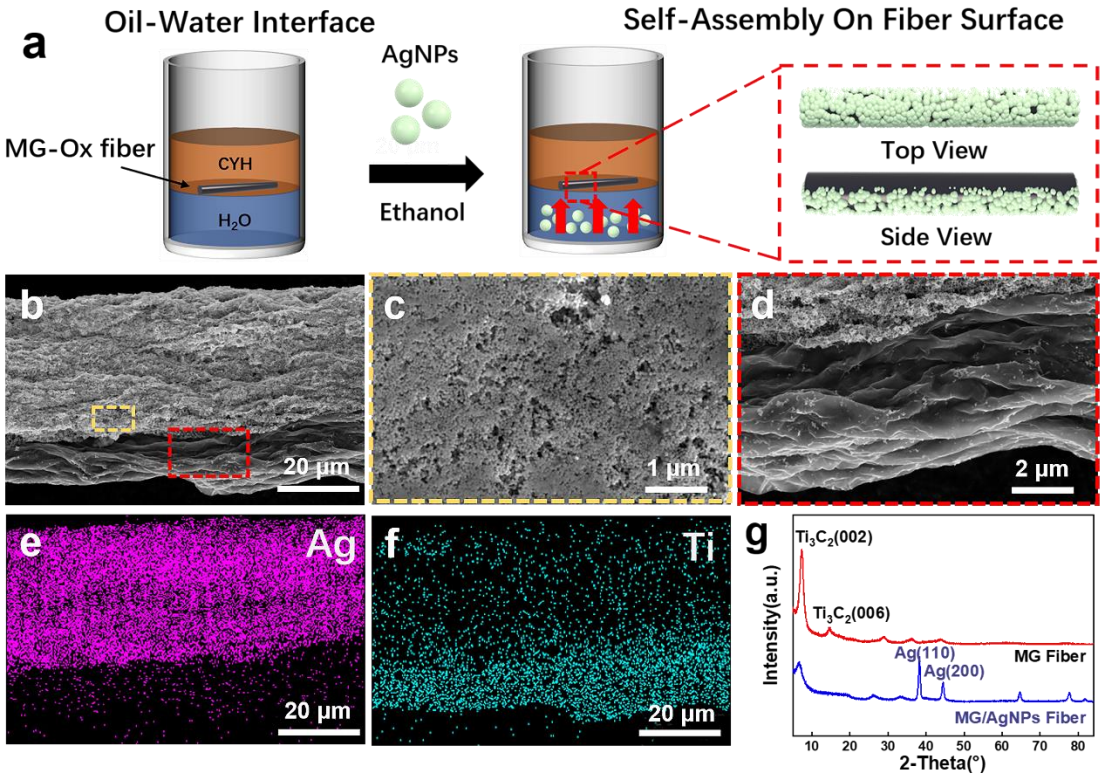

Figure 2. Construction of plasmonic hotspots on the fiber surface via self-assembly at the oil-water interface. (a) Schematic illustration of self-assembled AgNPs on the surface of MG-Ox fiber. (b) SEM image of MG/AgNPs fiber and (c) their corresponding high magnification images of Ag assembled nanostructure and almost no AgNPs, which are circled by yellow and red rectangles, respectively. (e) and (f) are the EDS mapping of (b) for Ag and Ti elements. (g) XRD pattern of MG/AgNPs fiber.

Figure 2a illustrates the schematic fabrication of the assembly process of the AgNPs on the surface of MG-Ox fiber, where the fiber can be used to stabilize and provide sites for the self-assembly of AgNPs. As a result, a Janus MG/AgNPs fiber

substrate was fabricated at the oil-water interface (**Figure 2b**). In bottom side at water phase, the dense and homogeneous AgNPs assembled on the surface of the fiber (**Figure 2c**) while almost no AgNPs were anchored on the upside of the fiber immersed in cyclohexane solution (**Figure 2d**). The formed Ag nanostructures on the MG fiber are verified by the energy dispersive spectroscopy (EDS) mapping of Ag and Ti (**Figure 2e** and **f)**. Thus, the formed Janus MG/AgNPs fiber substrate could be an excellent candidate for SERS sensing because it not only improves the SERS signals for target molecules via the strong electromagnetic field between the nearby AgNPs but also reduces the cost of SERS substrate from the half-covered AgNPs. In fact, as shown in **Figure S6**, full-covered AgNPs can be also constructed by multiple assemblies, which suggests that this self-assembly method could tailor full-covered or Janus structures as required. Furthermore, the XRD patterns of the partially covered AgNPs on the surface of fibers present two new strong peaks at 38.21° and 44.5°, which match well with the (111) and (200) facets of AgNPs (**Figure 2g),** further confirming the successful assembly of AgNPs on the MG fiber. Moreover, the XPS was performed for the MG/AgNPs-PVP fiber to analysis the binding of AgNPs and MG. As shown in **Figure S7a**, compared to the MG-Ox fiber, the characteristic peak at 364.2 eV in the total spectrum of the MG/AgNPs-PVP fiber was attributed to Ag 3d, suggesting the successful binding of AgNPs and MG fiber. Furthermore, the high-resolution spectrum of Ti 2p collected from MG/AgNPs-PVP fiber showed little change from MG-Ox surface (**Figure S7b**), demonstrating that the interaction of AgNPs and MG fibers mainly from electrostatic adsorption and no new chemical bonding created. This conclusion was also supported by the high-resolution spectrum of Ag 3d collected from MG/AgNPs-PVP (**Figure S7c**).

The type of surface functional groups on AgNPs is an important parameter for tuning the density of plasmonic hot spots on the fiber surface since the electrostatic effects of the functional groups determine the ability of AgNPs to assemble at the oil-water interface and the binding force with the fiber surface. Therefore, to achieve the best assembly strategy and the strongest plasmonic coupling, the assembly ability on the fiber surface of AgNPs with different surface functional groups and SERS

performance were investigated. As shown in **Figure 3a-h**, the SEM images clearly show the assembly behavior of AgNPs with different surface functional groups (Br-, trisodium citrate-TSC, polyvinyl pyrrolidone-PVP and cetyltrimethyl ammonium bromide-CTAB) on the bottom surface of fibers within water phase, which are noted as MG/AgNPs-Br, MG/AgNPs-TSC, MG/AgNPs-PVP and MG/AgNPs-CTAB fiber substrates respectively. Due to the negative zeta potential for both Br-capped AgNPs (-37.70 mV) and MXene (-42.01 mV) (**Figure 3i**), it is unfavorable for AgNPs to form a continuous monolayer plasmonic nanostructure on the MG fiber due to electrostatic repulsion.

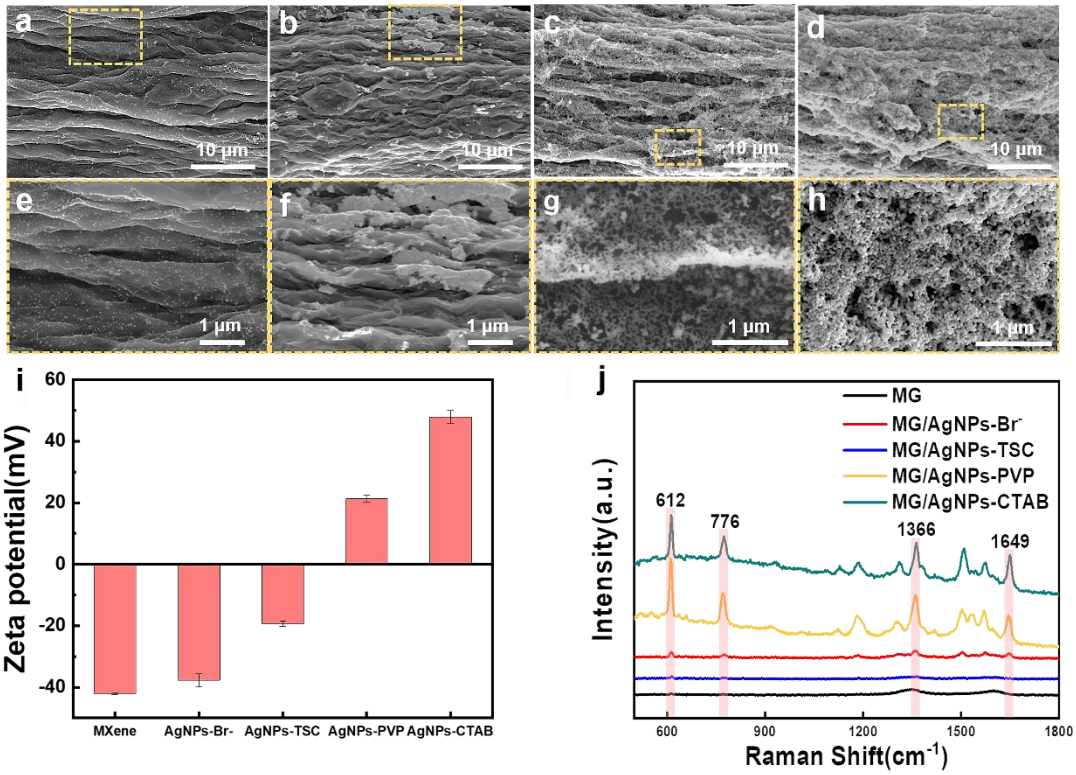

Figure 3. (a-d) SEM images of the bottom side of MG-Ox fibers functionalized by different groups within water phase: (a) Br-, (b) TSC, (c) PVP and (d) CTAB, and (e-h) their corresponding high magnification images of typical areas in (a-d) circled by yellow rectangle, respectively. (i) Zeta potential of MXene and AgNPs capped with functional groups. (j) SERS spectra of R6G collected from the surface of MG, MG/AgNPs-Br, MG/AgNPs-TSC, MG/AgNPs-PVP and MG/AgNPs-CTAB fiber substrates.

Thus, the sparse AgNPs are found on the surface of MG fiber (**Figure 3a and e**). The same phenomenon can be observed for the assembly of TSC-capped AgNPs (-

19.36 mV) on fiber in spite of some agglomeration of AgNPs (**Figure 3b and f**). In contrast, PVP- and CTAB-capped AgNPs with positive zeta potential (21.31 mV and 47.93 mV, respectively) can form dense and continuous plasmonic nanostructures on the fiber due to the effect of electrostatic adsorption between the MXene and those two functional AgNPs (**Figure 3c, d, g and h**). As a result, the uniform AuNPs nanostructures were aseembled on the surface of fiber substrate, which could provide a powerful Raman signal enhancement for target molecules.

To verify the efficiency of formed substrates, the SERS spectra of 10^{-8} M R6G collected from the surface of those four capped-fiber substrates were explored. As illustrated in **Figure 3j**, MG/AgNPs-PVP and MG/AgNPs-CTAB exhibit remarkable SERS performance, whereas only weak SERS signals can be found in the other two samples, indicating that the constructed AgNPs nanostructures on the fiber surface provide a huge electromagnetic (EM) enhancement for target molecules. Interestingly, although CTAB-capped AgNPs seem to form a denser film on the surface of MG-Ox fiber, the resultant SERS substrate exhibits a lower sensitivity for R6G molecules, compared to PVP-capped AgNPs (**Table S3**). This observation can be rationalized by the presence of compact bilayer supramolecular structure of CTAB that hinders the approach of R6G molecules to the surface of Ag NPs, thus affecting the photo-induced charge transfer (PICT) between MXene and the analytes[33, 48, 49]. Therefore, MG/AgNPs-PVP fiber is considered to be the optimal sample for building the high-performance flexible SERS substrate, where the MXenen nanosheets within the MG fiber could provide an additional signal enhancement of approximately 10^2 by PICT apart from the EM enhancement from the AgNPs nanostructures. Considering the flexibility and scalability of fiber substrate, MG/AgNPs-PVP fibers show great potential for on-site rapid testing and chemical analysis.

To evaluate the SERS performance of the MG/AgNPs-PVP fiber, the universal SERS probe molecule (R6G) was used as a model analyte. **Figure 4a** shows the SERS spectra of R6G at different concentrations ranging from 1×10^{-6} M to 1×10^{-15} M collected from the fiber surface. Four typical Raman characteristic peaks at 612, 772, 1362 and 1648 cm^{-1} could be clearly observed at each concentration, and the EF was

calculated as 1.53×10^{12} (see details in **Supporting Information Section 1**). Surprisingly, even at concentrations as low as femtomolar levels (10^{-15} M), 612 and 772 cm^{-1} characteristic peaks of R6G with excellent signal-to-noise ratios can still be observed from the fiber surface (**Figure 4b**), which is much lower than most previous reports [38-41]. Furthermore, the relationship between the intensity of the 612 cm^{-1} peak and the logarithm of the R6G concentration is highly correlated (**Figure S8**) with 0.991 correlation coefficient (R^2) in the concentration range of 10^{-6} M to 10^{-15} M. These results illustrate that the MG/AgNPs-PVP flexible fiber has excellent detection sensitivity and quantitative capability, providing favorable conditions for the wide application of SERS substrates.

In addition to the outstanding sensitivity and quantitative capability, reliable flexible SERS sensors also need high reproducibility and uniformity of Raman signals. **Figure 4c** shows the SERS signals of R6G collected from 10 sites on five different batches (2 sites for each batch) of MG/AgNPs-PVP fiber to explore their reproducibility. The SERS signal of 10^{-8} M R6G on different batches of fibers only displays minor fluctuations (**Figure S9**), which indicated the repeatability of fiber substrate. Moreover, to further illustrate the uniformity of MG/AgNPs-PVP fiber, 612 cm^{-1} peak intensities (10^{-8} M R6G) of R6G molecules at 200 random points were collected by Raman mapping in the 10×10 μm^2 area (**Figure S10**). The statistical results show that the relative standard deviation (RSD) of 9.47% is far lower than that of commercial substrates and other reported flexible SERS substrates[41, 50, 51] (**Figure 4d**), attributing to the uniform adsorption of target molecules on MG/AgNPs-PVP fiber substrate [31, 52]. Moreover, the stabilities of MG/AgNPs-PVP fiber with different storage time in air were also explored. From **Figure 4e** and **S11**, the MG/AgNPs-PVP fiber maintains 83.7% signal intensity of fresh sample after 60 days of storage, whereas the corresponding AgNPs-PVP colloids coated on SiO_2 only maintain 52.3%, indicating that the produced AgNPs anchored on MG fiber have a longer service life. This could be attributed to the additional CT effect provided by the acidified MG substrate in the MG/AgNPs-PVP fiber, which buffers the deterioration in SERS performance caused by the oxidation of AgNPs. These exciting results show that the

MG/AgNPs-PVP fiber hold promise as a sensitive, reliable, and flexible SERS sensors for practical applications.

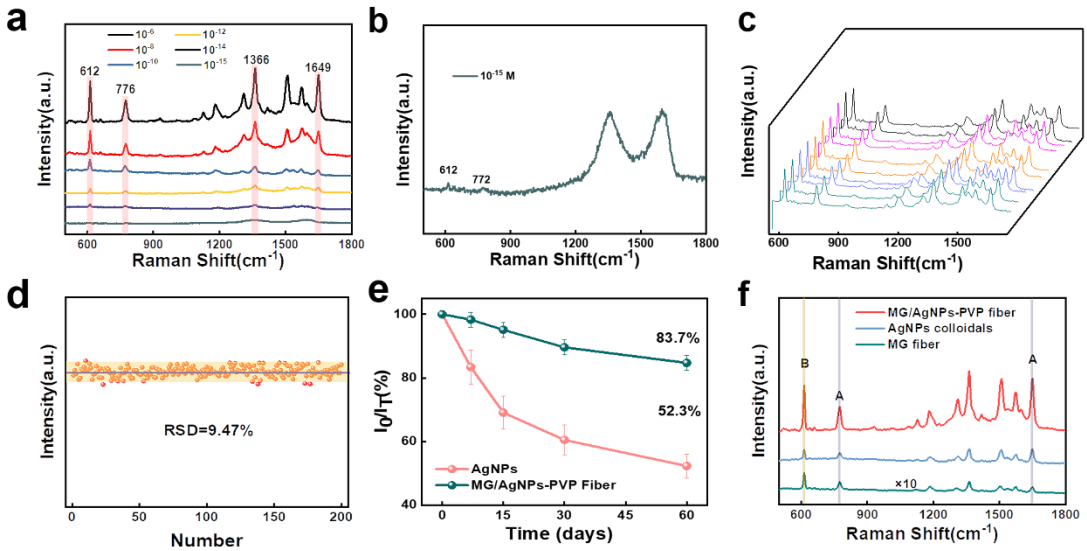

Figure 4. (a) SERS spectra of R6G molecules from 1×10^{-6} to 1×10^{-15} M collected on MG/AgNP-PVP fiber and (b) the corresponding enlarge view of 10^{-15} M R6G. (c) Stability of Raman signals of R6G located on MG/AgNPs-PVP fiber produced from five batches. (d) RSD of Raman signal intensity at 612 cm^{-1} of R6G collected from 200 random spots on fiber. (e) Attenuation of Raman signal intensity at 612 cm^{-1} versus storage time of MG/AgNPs-PVP fiber and their AgNPs-PVP colloids. (f) SERS spectra of R6G collected from MG fiber, monolayer AgNPs nanostructure and MG/AgNPs-PVP fiber. Note: For the facile comparison, the signal of R6G on the MG fiber in (f) was amplified 10 times.

To explore the underlying SERS mechanism of MG/AgNPs-PVP fiber, the enhanced Raman spectra of R6G (10^{-8} M) were collected from AgNPs colloids, MG and MG/AgNPs-PVP fibers respectively. For R6G molecules, the peak at 612 cm^{-1} is attributed to the asymmetric mode (in-plane C-C-C ring, B2), while the peak at 1648 cm^{-1} belongs to the symmetric mode (in-plane C-C stretching vibrations, A1) [32, 53]. According to the unified theory of SERS proposed by Lombardi[54], the A1 mode intensity can only be enhanced by the electromagnetic field enhancement (EM), while the B2 mode intensity can be selectively enhanced through a charge-transfer (CT) mechanism. In other words, the ratio of the relative intensities of peak B2 to peak A1 (I_B/I_A for short) reflects the contribution of CT to the total Raman signal enhancement.

As demonstrated in **Figure 4f**, the value of I_B/I_A for MG fiber$>I_B/I_A$ for MG/AgNPs-PVP fiber $>I_B/I_A$ for AgNPs colloids. It reveals that the SERS signal collected on MG/AgNPs-PVP fiber is mainly from synergistic enhancement of produced AgNPs nanostructure (EM) and the CT between MXene and R6G molecules (CM) [33, 48]. Here, the CT effect is further verified by the UV spectra of the mixture of MXene/R6G and AgNPs/R6G with their corresponding R6G solution respectively**. Figure S12** demonstrates that the main absorption peak of R6G mixed with MXene exhibited a red-shift from 526 to 543 nm, whereas no shift was observed in R6G mixed with AgNPs. It suggests that the contribution of AgNPs nanostructures to the Raman signal intensity enhancement is mainly dominated by EM, while CT effect is almost deriving from MXene nansheets within MG fiber. Thus, all results indicate that the Raman enhancement mechanism of R6G molecules on MG/AgNPs-PVP fiber is derived from the combined enhancement of EM and CT.

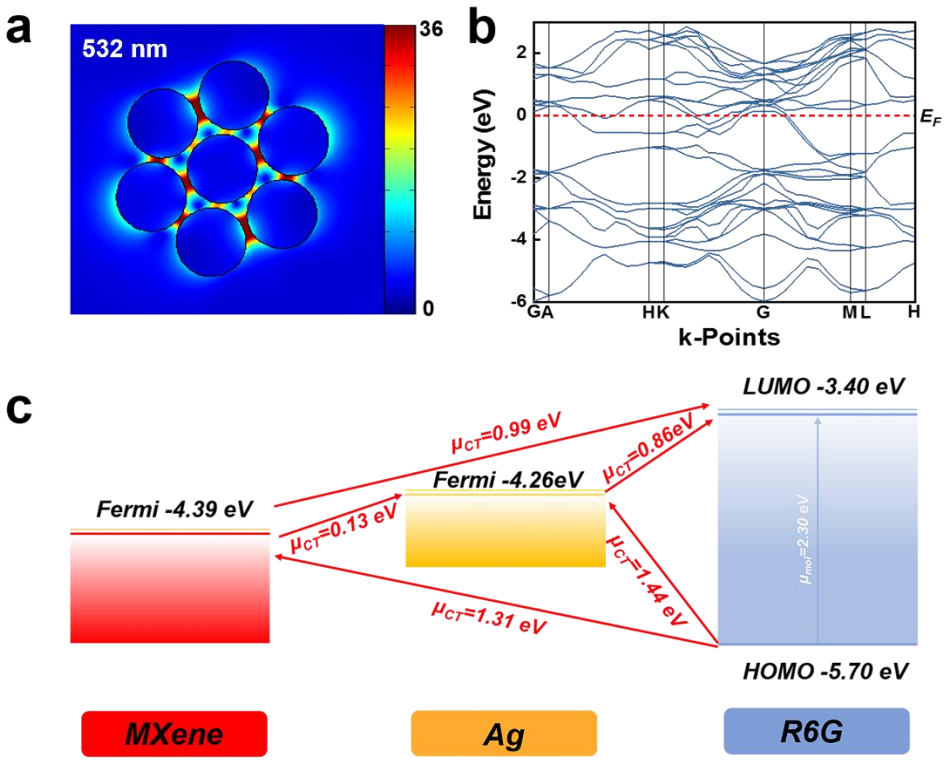

Figure 5. (a) Electric field distribution of monolayer AgNPs nanostructure on MG fiber. (b) Band structure of MXene. (c) Schematic illustration of the CT process between MG/AgNPs-PVP fiber and R6G molecules.

Furthermore, the distribution of the electromagnetic field generated by the plasmonic nanostructures on the fiber was numerically simulated by FEM (see details in **Experimental Part**). **Figure 5a** shows the hot spot distribution of AgNPs placed on MG fiber under an incident field intensity of E_0=1, where the strongest hot spots are uniformly and densely distributed in the gaps of AgNPs nanostructures. Notably, the intensity of the electromagnetic field at the "hot spot" is amplified by 38 times (E_{max}=38). Since the contribution of EM to the enhancement factor (EF) can be described as $EF \approx \left|\frac{E_{max}}{E_0}\right|^4$, the EM contribution can be calculated to be 4.05×10^7.

Moreover, the contribution of CT to EF was investigated by Herzberg-Teller rules [54, 55]. According to Fermi's golden rule, the electron transition probability rate can be expressed as $\omega_{lk=}\frac{2\pi}{\hbar}g(E_k)|H'_{kl}|$, where $\hbar$ is Planck's constant, $g(E_k)$ is the DOS of the substrate, and $|H'_{kl}|$ is the element of the matrix associated with the HOMO and LUMO of the analyte and the energy levels of the SERS substrate. The energy band structure and DOS of MXene were calculated by DTF as shown in **Figure 5b** and **S13**. MXene has abundant free electrons near the Fermi level, which provides favorable conditions for CT resonance-enhanced Raman signals. **Figure 5c** schematically illustrates the possible CT paths between MG/AgNPs-PVP fiber and R6G molecules. The intermolecular transitions (μ_{mol}) and charge transfer transitions (μ_{CT}) could be thus happened under the illustration of laser light at 532 nm (2.33 eV), due to the Fermi level of the MG-Ox fiber and AgNPs located at -4.08 and -4.26 eV and the LUMO and HOMO of R6G placed at -3.40 and -5.70 eV (**Figure 5c**). These effects enables the SERS signal of R6G substantially enhanced via the CT resonance from intramolecular, substrate-to-molecular or molecular-to-substrate mechanism. Furthermore, owing to the excellent electron acceptance and shuttling capability of AgNPs, the produced substrate can effectively reduce reverse transfer, which further increases the polarization tensor of the R6G molecule[56].

Table 1. The LOD of Thiram in previously reported and this work

Material	LOD	with flexibility	Ref.
PDMS-AgNRs	10^{-7} M	Yes	[22]
AuNPs Tape	2.6×10^{-5} M	Yes	[24]
Au@AgNPs-MOF	3.1×10^{-8} M	No	[21]
GO/AgNPs	5×10^{-9} M	Yes	[50]
AgNP@AgNW-PDMS	10^{-10} M	Yes	[27]
AuNRs	10^{-11} M	No	[23]
MG/AgNPs-PVP	10^{-11} M	Yes	This Work

Pesticides and insecticides such as thiuram, thiabendazole and tymetrozine are widely used in agricultural production to prevent pests. However, pesticide residues on crop surfaces ingested by humans can cause severe health problems like cancer[57, 58]. Here, the limit of detection (LOD) and quantitative ability of MG/AgNPs-PVP fiber was evaluated for thiuram, thiabendazole and tymetrozine molecules. Impressively, the characteristic peaks of the three pesticides can be clearly identified in the concentration range from 10^{-7} to 10^{-11}M (**Figure 6a-c**), and the LOD is much lower than the permissible limit (7 ppm, 2.9×10^{-5} M) and other SERS substrates (**Table 1**). The relationship between the intensity of the characteristic peaks and the logarithm of the concentrations of three pesticides were fitted by a linear function with R^2 values of 0.981, 0991 and 0.972 (**Figure S14**) respectively. Thus, as shown in **Figure S15a-c**, based on the wide detection ranges and accurate quantitative capability of MG/AgNPs-PVP fiber, the positions and relative intensity of the respective characteristic peaks were extracted from the SERS spectra of those three molecules, and subsequently the results were converted into color barcodes (see details in **Experimental Part**). These color barcodes are easier to read and understand than complex Raman spectra and are expected to be combined with barcode scanners for the rapid screening of pesticide residues.

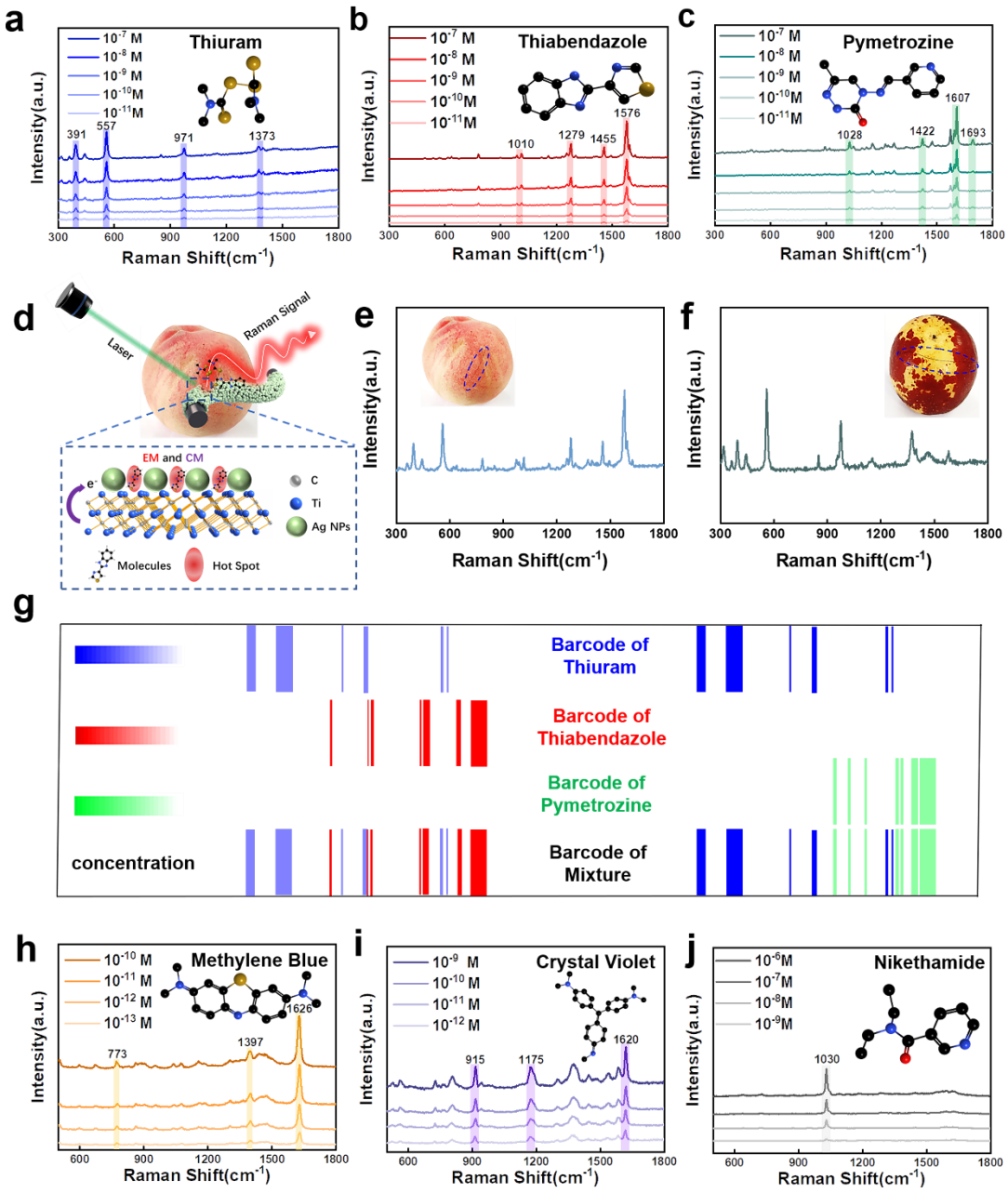

Figure 6. Label-free detection of flexible of MG/AgNPs-PVP fiber substrate. The SERS detection of (a) thiuram, (b) thiabendazole and (c) pymetrozine molecules from 10^{-7} to 10^{-11} M. (d) Schematic diagram of multiplexed pesticide detection from flexible MG/AgNPs-PVP fiber. SERS spectrum of the mixed pesticides on the surface of (e) peach and (f) winter jujube. (g) The individual barcodes for each pesticide and the superimposed barcodes for the mixed pesticides. The SERS spectra collected from (h) methylene blue, (i) crystal violet and (j) nikethamide.

In agricultural production, mixed pesticides are often used to improve the killing efficiency of pests, thus it critical to achieve the detection of multiple residues on the crop surface. As a proof-of-concept test, bi-components of pesticide residues on fruit

peels were used to verify the feasibility of MG/AgNPs-PVP fiber substrate for the SERS detection. As demonstrated in **Figure 6d**, the flexible fiber can easily absorb pesticide molecules from the surface of pesticides/ethanol solution moistened peels and collect Raman signals with high sensitivity from the synergistic effect of the excited charge-transfer (CT) resonance from MG fiber and large electromagnetic (EM) field enhancement from assembled AgNPs.

For instance, SERS spectra of the mixed pesticides thiuram-thiabendazole (**Figure 6e**) and thiuram-pymetrozine (**Figure 6f**) were collected from peach and winter jujube peels. The SERS signal of the mixed pesticides contains a large amount of molecular fingerprint information and some unobtrusive vibrational signals which make it difficult to achieve rapid multiplexed detection from the mixtures. To circumvent this issue, the composition and concentration of each pesticide were used to construct color barcode for analyzing the signal intensities of mixed pesticides (**Figure S15** and **Table S4**). By comparing the color barcode of each pesticide molecules, information on the concentration and composition of the pesticide mixture can be easily obtained with the error <7.3% (**Figure 6g**). Moreover, as a versatile label-free sensor, the flexible MG/AgNPs-PVP fiber can also recognize target molecules in a wide range of fields with excellent quantitative capabilities (**Figure S16**), such as methylene blue (MB, an organic pollutant, **Figure 6h**), crystal violet (CV, a fish drug, **Figure 6i**) and nikethamide (NTA, a prohibited stimulant, **Figure 6j**). With the construction of more standard color barcodes, the produced flexible MG/AgNPs-PVP fiber is expected to serve as powerful SERS sensors for the rapid analysis in real samples.

4. Conclusion

In conclusion, we developed an unique oil-water interface self-assemble strategy to construct a label-free flexible SERS sensor for the rapid multiplexed analysis of versatile target molecules. As shown by the SERS experiments and theoretical simulations, MG/AgNPs-PVP fiber substrate exhibited a low detection limit (1×10^{-15} M), outstanding sensitivity (EF=1.53×10^{12}) and high stability (RSD=9.47%, over 60

days for storage at RT) for R6G molecules, owing to the dense and uniform electromagnetic hot spots from AgNPs nanostructures and the effective CT of MG fiber and R6G. Moreover, by virtue of the flexibility and scalability of fiber substrate, rapid multiplexed sensing of pesticide residues in fruit peels can be achieved with an error <7.3%. Meanwhile, the standard color barcode library was constructed by SERS spectra related to pesticide molecular concentrations to support rapid screening of a large range of real samples. Moreover, the constructed fiber sensor also demonstrates a versatile capacity for detecting of other industrially relevant compounds, such as MB, CV and NTA. We envision that this work could provide new insights into the design and fabrication of high-performance flexible SERS sensors for multiplexed label-free detection and demonstrate the potential of SERS technology for large-scale rapid screening in real world scenarios.

Supporting Information:

Supporting Information is available from the XXX or from the author.

Conflict of Interest:

The authors declare no conflict of interest.

Author contributions:

X. L. and A. D. conceived the idea and designed the experiments. X. L. performed the experiments. Y. S., W. D., B. W., Y. L., S. W. and T. Z. helped with the experiments. A. D. and T. L. supervised the work. X. L., A.D., A. Z., T. C. L. and Y. Y. drafted the manuscript, and all the authors contributed to the editing of the manuscript.

Acknowledgments:

We acknowledge support by the Natural Science Foundation of China (52072302, 51802267, 51872235), the Science and Technology Plan Project from Xi'an (22GXFW0135), and the China Postdoctoral Science Foundation (2020M673475).

References

[1] N. Reyes-Garcés, E. Gionfriddo, G.A. Gómez-Ríos, M.N. Alam, E. Boyacı, B. Bojko, et al., Advances in Solid Phase Microextraction and Perspective on Future Directions, Analytical Chemistry, 90(2018) 302-60. https://doi.org/10.1021/acs.analchem.7b04502

[2] Y. Jiang, D.-W. Sun, H. Pu, Q. Wei, Surface enhanced Raman spectroscopy (SERS): A novel reliable technique for rapid detection of common harmful chemical residues, Trends in Food Science & Technology, 75(2018) 10-22. https://doi.org/https://doi.org/10.1016/j.tifs.2018.02.020

[3] D. Goulson, Pesticides linked to bird declines, Nature, 511(2014) 295-6. https://doi.org/10.1038/nature13642

[4] R.W. Taylor, T.-C. Lee, O.A. Scherman, R. Esteban, J. Aizpurua, F.M. Huang, et al., Precise Subnanometer Plasmonic Junctions for SERS within Gold Nanoparticle Assemblies Using Cucurbit[n]uril "Glue", ACS Nano, 5(2011) 3878-87. https://doi.org/10.1021/nn200250v

[5] M.-L. Xu, J.-B. Liu, J. Lu, Determination and Control of Pesticide Residues in Beverages: A Review of Extraction Techniques, Chromatography, and Rapid Detection Methods, Applied Spectroscopy Reviews, 49(2014) 97-120. https://doi.org/10.1080/05704928.2013.803978

[6] E. Watanabe, S. Miyake, Y. Yogo, Review of Enzyme-Linked Immunosorbent Assays (ELISAs) for Analyses of Neonicotinoid Insecticides in Agro-environments, Journal of Agricultural and Food Chemistry, 61(2013) 12459-72. https://doi.org/10.1021/jf403801h

[7] J. Langer, D. Jimenez de Aberasturi, J. Aizpurua, R.A. Alvarez-Puebla, B. Auguié, J.J. Baumberg, et al., Present and Future of Surface-Enhanced Raman Scattering, ACS Nano, 14(2020) 28-117. https://doi.org/10.1021/acsnano.9b04224

[8] M.-L. Xu, Y. Gao, X.X. Han, B. Zhao, Detection of Pesticide Residues in Food Using Surface-Enhanced Raman Spectroscopy: A Review, Journal of Agricultural and Food Chemistry, 65(2017) 6719-26. https://doi.org/10.1021/acs.jafc.7b02504

[9] A. Bernat, M. Samiwala, J. Albo, X. Jiang, Q. Rao, Challenges in SERS-based pesticide detection and plausible solutions, Journal of Agricultural and Food Chemistry, 67(2019) 12341-7. https://doi.org/10.1021/acs.jafc.9b05077

[10] A. Dang, Y. Wang, H. Zhang, W. Panatdasirisuk, Y. Xia, Z. Wang, et al., Electrospun Gold Nanoprism/Poly(vinyl alcohol) Nanofibers for Flexible and Free-Standing Surface-Enhanced Raman Scattering Substrates, ACS Applied Nano Materials, 5(2022) 6650-8. https://doi.org/10.1021/acsanm.2c00689

[11] W.-I.K. Chio, H. Xie, Y. Zhang, Y. Lan, T.-C. Lee, SERS biosensors based on cucurbituril-mediated nanoaggregates for wastewater-based epidemiology, TrAC Trends in Analytical Chemistry, 146(2022) 116485. https://doi.org/https://doi.org/10.1016/j.trac.2021.116485

[12] H.-H. Jeong, E. Choi, E. Ellis, T.-C. Lee, Recent advances in gold nanoparticles for biomedical applications: from hybrid structures to multi-functionality, Journal of Materials Chemistry B, 7(2019) 3480-96. https://doi.org/10.1039/C9TB00557A

[13] G. Davison, T. Jones, J. Liu, J. Kim, Y. Yin, D. Kim, et al., Computer-Aided Design and Analysis of Spectrally Aligned Hybrid Plasmonic Nanojunctions for SERS

Detection of Nucleobases, Advanced Materials Technologies, n/a(2023) 2201400.https://doi.org/https://doi.org/10.1002/admt.202201400
[14] W.J. Peveler, H. Jia, T. Jeen, K. Rees, T.J. Macdonald, Z. Xia, et al., Cucurbituril-mediated quantum dot aggregates formed by aqueous self-assembly for sensing applications, Chemical Communications, 55(2019) 5495-8.https://doi.org/10.1039/C9CC00410F
[15] P.D. Howes, R. Chandrawati, M.M. Stevens, Colloidal nanoparticles as advanced biological sensors, Science, 346(2014) 1247390.https://doi.org/doi:10.1126/science.1247390
[16] W.-I.K. Chio, J. Liu, T. Jones, J. Perumal, U.S. Dinish, I.P. Parkin, et al., SERS multiplexing of methylxanthine drug isomers via host–guest size matching and machine learning, Journal of Materials Chemistry C, 9(2021) 12624-32.https://doi.org/10.1039/D1TC02004H
[17] J. Homola, Surface Plasmon Resonance Sensors for Detection of Chemical and Biological Species, Chemical Reviews, 108(2008) 462-93.https://doi.org/10.1021/cr068107d
[18] W.-I.K. Chio, W.J. Peveler, K.I. Assaf, S. Moorthy, W.M. Nau, I.P. Parkin, et al., Selective Detection of Nitroexplosives Using Molecular Recognition within Self-Assembled Plasmonic Nanojunctions, The Journal of Physical Chemistry C, 123(2019) 15769-76.https://doi.org/10.1021/acs.jpcc.9b02363
[19] H.K. Lee, Y.H. Lee, C.S.L. Koh, G.C. Phan-Quang, X. Han, C.L. Lay, et al., Designing surface-enhanced Raman scattering (SERS) platforms beyond hotspot engineering: emerging opportunities in analyte manipulations and hybrid materials, Chemical Society Reviews, 48(2019) 731-56.https://doi.org/10.1039/C7CS00786H
[20] Y. Xu, F.Y.H. Kutsanedzie, M. Hassan, J. Zhu, W. Ahmad, H. Li, et al., Mesoporous silica supported orderly-spaced gold nanoparticles SERS-based sensor for pesticides detection in food, Food Chemistry, 315(2020) 126300.https://doi.org/https://doi.org/10.1016/j.foodchem.2020.126300
[21] H. Lai, H. Dai, G. Li, Z. Zhang, Rapid determination of pesticide residues in fruit and vegetable using Au@AgNPs decorated 2D Ni-MOF nanosheets as efficient surface-enhanced Raman scattering substrate, Sensors and Actuators B: Chemical, 369(2022) 132360.https://doi.org/https://doi.org/10.1016/j.snb.2022.132360
[22] S. Kumar, P. Goel, J.P. Singh, Flexible and robust SERS active substrates for conformal rapid detection of pesticide residues from fruits, Sensors and Actuators B: Chemical, 241(2017) 577-83.https://doi.org/https://doi.org/10.1016/j.snb.2016.10.106
[23] B. M. B, R.P. B, A. Tripathi, S. Yadav, N.S. John, R. Thapa, et al., A Unique Bridging Facet Assembly of Gold Nanorods for the Detection of Thiram through Surface-Enhanced Raman Scattering, ACS Sustainable Chemistry & Engineering, 10(2022) 7330-40.https://doi.org/10.1021/acssuschemeng.2c01089
[24] J. Chen, Y. Huang, P. Kannan, L. Zhang, Z. Lin, J. Zhang, et al., Flexible and Adhesive Surface Enhance Raman Scattering Active Tape for Rapid Detection of Pesticide Residues in Fruits and Vegetables, Analytical Chemistry, 88(2016) 2149-55.https://doi.org/10.1021/acs.analchem.5b03735

[25] Z. Li, X. Huang, G. Lu, Recent developments of flexible and transparent SERS substrates, Journal of Materials Chemistry C, 8(2020) 3956-69. https://doi.org/10.1039/D0TC00002G
[26] K. Xu, R. Zhou, K. Takei, M. Hong, Toward Flexible Surface-Enhanced Raman Scattering (SERS) Sensors for Point-of-Care Diagnostics, Advanced Science, 6(2019) 1900925. https://doi.org/https://doi.org/10.1002/advs.201900925
[27] W. Wei, Y. Du, L. Zhang, Y. Yang, Y. Gao, Improving SERS hot spots for on-site pesticide detection by combining silver nanoparticles with nanowires, Journal of Materials Chemistry C, 6(2018) 8793-803. https://doi.org/10.1039/C8TC01741G
[28] Y. Fang, N.-H. Seong, D.D. Dlott, Measurement of the Distribution of Site Enhancements in Surface-Enhanced Raman Scattering, Science, 321(2008) 388-92. https://doi.org/10.1126/science.1159499
[29] Y. Peng, C. Lin, L. Long, T. Masaki, M. Tang, L. Yang, et al., Charge-Transfer Resonance and Electromagnetic Enhancement Synergistically Enabling MXenes with Excellent SERS Sensitivity for SARS-CoV-2 S Protein Detection, Nano-Micro Letters, 13(2021) 52. https://doi.org/10.1007/s40820-020-00565-4
[30] B. Soundiraraju, B.K. George, Two-Dimensional Titanium Nitride (Ti2N) MXene: Synthesis, Characterization, and Potential Application as Surface-Enhanced Raman Scattering Substrate, ACS Nano, 11(2017) 8892-900. https://doi.org/10.1021/acsnano.7b03129
[31] K. Yang, K. Zhu, Y. Wang, Z. Qian, Y. Zhang, Z. Yang, et al., Ti3C2Tx MXene-Loaded 3D Substrate toward On-Chip Multi-Gas Sensing with Surface-Enhanced Raman Spectroscopy (SERS) Barcode Readout, ACS Nano, 15(2021) 12996-3006. https://doi.org/10.1021/acsnano.1c01890
[32] Z. He, T. Rong, Y. Li, J. Ma, Q. Li, F. Wu, et al., Two-Dimensional TiVC Solid-Solution MXene as Surface-Enhanced Raman Scattering Substrate, ACS Nano, 16(2022) 4072-83. https://doi.org/10.1021/acsnano.1c09736
[33] A. Sarycheva, T. Makaryan, K. Maleski, E. Satheeshkumar, A. Melikyan, H. Minassian, et al., Two-Dimensional Titanium Carbide (MXene) as Surface-Enhanced Raman Scattering Substrate, The Journal of Physical Chemistry C, 121(2017) 19983-8. https://doi.org/10.1021/acs.jpcc.7b08180
[34] M. Han, K. Maleski, C.E. Shuck, Y. Yang, J.T. Glazar, A.C. Foucher, et al., Tailoring Electronic and Optical Properties of MXenes through Forming Solid Solutions, Journal of the American Chemical Society, 142(2020) 19110-8. https://doi.org/10.1021/jacs.0c07395
[35] Y. Gogotsi, B. Anasori, The Rise of MXenes, ACS Nano, 13(2019) 8491-4. https://doi.org/10.1021/acsnano.9b06394
[36] M. Naguib, M. Kurtoglu, V. Presser, J. Lu, J. Niu, M. Heon, et al., Two-Dimensional Nanocrystals Produced by Exfoliation of Ti3AlC2, Advanced Materials, 23(2011) 4248-53. https://doi.org/https://doi.org/10.1002/adma.201102306
[37] A. Dang, Y. Sun, Y. Liu, Y. Xia, X. Liu, Y. Gao, et al., Flexible Ti3C2Tx/Carbon Nanotubes/CuS Film Electrodes Based on a Dual-Structural Design for High-Performance All-Solid-State Supercapacitors, ACS Applied Energy Materials, 5(2022) 9158-72. https://doi.org/10.1021/acsaem.2c01738

[38] R. Cheng, T. Hu, M. Hu, C. Li, Y. Liang, Z. Wang, et al., MXenes induce epitaxial growth of size-controlled noble nanometals: A case study for surface enhanced Raman scattering (SERS), Journal of Materials Science & Technology, 40(2020) 119-27. https://doi.org/https://doi.org/10.1016/j.jmst.2019.09.013
[39] L. Liu, C. Shangguan, J. Guo, K. Ma, S. Jiao, Y. Yao, et al., Ultrasensitive SERS Detection of Cancer-Related miRNA-182 by MXene/MoS2@AuNPs with Controllable Morphology and Optimized Self-Internal Standards, Advanced Optical Materials, 8(2020) 2001214. https://doi.org/https://doi.org/10.1002/adom.202001214
[40] R. Liu, L. Jiang, Z. Yu, X. Jing, X. Liang, D. Wang, et al., MXene (Ti3C2Tx)-Ag nanocomplex as efficient and quantitative SERS biosensor platform by in-situ PDDA electrostatic self-assembly synthesis strategy, Sensors and Actuators B: Chemical, 333(2021) 129581. https://doi.org/https://doi.org/10.1016/j.snb.2021.129581
[41] H. Xie, P. Li, J. Shao, H. Huang, Y. Chen, Z. Jiang, et al., Electrostatic Self-Assembly of Ti3C2Tx MXene and Gold Nanorods as an Efficient Surface-Enhanced Raman Scattering Platform for Reliable and High-Sensitivity Determination of Organic Pollutants, ACS Sensors, 4(2019) 2303-10. https://doi.org/10.1021/acssensors.9b00778
[42] X. Liu, A. Dang, T. Li, Y. Sun, T.-C. Lee, W. Deng, et al., Plasmonic Coupling of Au Nanoclusters on a Flexible MXene/Graphene Oxide Fiber for Ultrasensitive SERS Sensing, ACS Sensors, (2023). https://doi.org/10.1021/acssensors.2c02808
[43] Q. Yang, Z. Xu, B. Fang, T. Huang, S. Cai, H. Chen, et al., MXene/graphene hybrid fibers for high performance flexible supercapacitors, Journal of Materials Chemistry A, 5(2017) 22113-9. https://doi.org/10.1039/C7TA07999K
[44] S. Meng, J. Liang, W. Jia, P. Zhang, Q. Su, C. Wang, et al., Metal-free and flexible surface-enhanced Raman scattering substrate based on oxidized carbon cloth, Carbon, 189(2022) 152-61. https://doi.org/https://doi.org/10.1016/j.carbon.2021.12.055
[45] R.B. Rakhi, B. Ahmed, M.N. Hedhili, D.H. Anjum, H.N. Alshareef, Effect of Postetch Annealing Gas Composition on the Structural and Electrochemical Properties of Ti2CTx MXene Electrodes for Supercapacitor Applications, Chemistry of Materials, 27(2015) 5314-23. https://doi.org/10.1021/acs.chemmater.5b01623
[46] C. Liang, Z.-A. Lu, M. Zheng, M. Chen, Y. Zhang, B. Zhang, et al., Band Structure Engineering within Two-Dimensional Borocarbonitride Nanosheets for Surface-Enhanced Raman Scattering, Nano Letters, 22(2022) 6590-8. https://doi.org/10.1021/acs.nanolett.2c01825
[47] S. Lin, H. Guan, Y. Liu, S. Huang, J. Li, W. Hasi, et al., Binary Plasmonic Assembly Films with Hotspot-Type-Dependent Surface-Enhanced Raman Scattering Properties, ACS Applied Materials & Interfaces, 13(2021) 53289-99. https://doi.org/10.1021/acsami.1c18565
[48] T.B. Limbu, B. Chitara, M.Y. Garcia Cervantes, Y. Zhou, S. Huang, Y. Tang, et al., Unravelling the Thickness Dependence and Mechanism of Surface-Enhanced Raman Scattering on Ti3C2TX MXene Nanosheets, The Journal of Physical Chemistry C, 124(2020) 17772-82. https://doi.org/10.1021/acs.jpcc.0c05143
[49] G. Davison, Y. Yin, T. Jones, I.P. Parkin, W.J. Peveler, T.-C. Lee, Multi-mode enhanced Raman scattering spectroscopy using aggregation-free hybrid metal/metal-

oxide nanoparticles with intrinsic oxygen vacancies, Journal of Materials Chemistry C, (2023). https://doi.org/10.1039/D2TC05069B
[50] Z. Cao, P. He, T. Huang, S. Yang, S. Han, X. Wang, et al., Plasmonic Coupling of AgNPs near Graphene Edges: A Cross-Section Strategy for High-Performance SERS Sensing, Chemistry of Materials, 32(2020) 3813-22. https://doi.org/10.1021/acs.chemmater.9b05293
[51] X. Liu, J. Ma, P. Jiang, J. Shen, R. Wang, Y. Wang, et al., Large-Scale Flexible Surface-Enhanced Raman Scattering (SERS) Sensors with High Stability and Signal Homogeneity, ACS Applied Materials & Interfaces, 12(2020) 45332-41. https://doi.org/10.1021/acsami.0c13691
[52] R. Zhang, J. Liu, Y. Li, MXene with Great Adsorption Ability toward Organic Dye: An Excellent Material for Constructing a Ratiometric Electrochemical Sensing Platform, ACS Sensors, 4(2019) 2058-64. https://doi.org/10.1021/acssensors.9b00654
[53] Y. Ge, F. Wang, Y. Yang, Y. Xu, Y. Ye, Y. Cai, et al., Atomically Thin TaSe2 Film as a High-Performance Substrate for Surface-Enhanced Raman Scattering, Small, 18(2022) 2107027. https://doi.org/https://doi.org/10.1002/smll.202107027
[54] J.R. Lombardi, R.L. Birke, A Unified Approach to Surface-Enhanced Raman Spectroscopy, The Journal of Physical Chemistry C, 112(2008) 5605-17. https://doi.org/10.1021/jp800167v
[55] J.R. Lombardi, R.L. Birke, A Unified View of Surface-Enhanced Raman Scattering, Accounts of Chemical Research, 42(2009) 734-42. https://doi.org/10.1021/ar800249y
[56] S. Guo, S. Jin, E. Park, L. Chen, Z. Mao, Y.M. Jung, Photo-Induced Charge Transfer Enhancement for SERS in a SiO2 – Ag – Reduced Graphene Oxide System, ACS Applied Materials & Interfaces, 13(2021) 5699-705. https://doi.org/10.1021/acsami.0c17056
[57] P. Nicolopoulou-Stamati, S. Maipas, C. Kotampasi, P. Stamatis, L. Hens, Chemical Pesticides and Human Health: The Urgent Need for a New Concept in Agriculture, Frontiers in Public Health, 4(2016). https://doi.org/10.3389/fpubh.2016.00148
[58] G. Van Maele-Fabry, A.-C. Lantin, P. Hoet, D. Lison, Residential exposure to pesticides and childhood leukaemia: A systematic review and meta-analysis, Environment International, 37(2011) 280-91. https://doi.org/https://doi.org/10.1016/j.envint.2010.08.016